

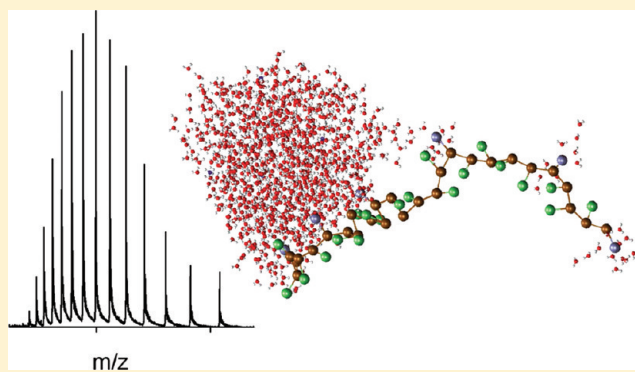
# Modeling the Behavior of Coarse-Grained Polymer Chains in Charged Water Droplets: Implications for the Mechanism of Electrospray Ionization

Elias Ahadi and Lars Konermann\*

Department of Chemistry, The University of Western Ontario, London, Ontario N6A 5B7, Canada

Supporting Information

**ABSTRACT:** The mechanism whereby macromolecular analytes are transferred into the gas phase during the final stages of electrospray ionization (ESI) remains a matter of debate. In this work, we employ molecular dynamics simulations to examine the temporal behavior of nanometer-sized aqueous ESI droplets containing a polymer chain and excess ammonium ions. The polymer is modeled using a coarse-grained framework where a bead-string backbone is decorated with side chains that can be nonpolar, cationic, or anionic. Polymers that adopt compact conformations and that carry a large number of charged side chains remain close to the droplet center, where the charges are extensively hydrated. The ESI process for these compact/hydrophilic macromolecules must involve solvent evaporation to dryness. This behavior is consistent with the charged residue model (CRM). A completely different scenario is encountered for disordered (extended) chains that carry a large number of nonpolar side chains. In this case, the macromolecule tends to be rapidly expelled from the droplet surface in a stepwise sequential fashion. This process produces metastable structures where one end of the extended polymer chain remains connected with the droplet via charge solvation. Disruption of these last interactions will then produce a free gas phase macromolecular ion. The data of this work imply that the ESI process for unfolded/hydrophobic polymers proceeds via an ion evaporation (IEM)-like mechanism that is facilitated by hydrophobic solute/solvent interactions. Our model predicts that the ESI efficiency of the latter scenario is considerably higher than for the CRM. This prediction is verified experimentally through ESI mass spectrometry measurements on myoglobin.



## INTRODUCTION

Electrospray ionization (ESI) produces intact gaseous ions from molecules in solution, thereby making them amenable to analysis by mass spectrometry (MS). ESI-MS can be applied to a wide range of chemical species, from low molecular weight compounds to large biopolymers. The formation of multiply charged ions during ESI facilitates the detection of high mass analytes on mass spectrometers with limited  $m/z$  range. Also, ESI allows the coupling of liquid-phase separations with MS analysis. The combination of these attractive features has made ESI-MS a versatile and widely used technique.<sup>1</sup>

During operation of a standard ESI source, micrometer-sized solvent droplets containing analyte and excess charge are emitted from the tip of a Taylor cone. Solvent evaporation increases the charge density on the droplets to the Rayleigh limit where surface tension and Coulomb repulsion are balanced. The net droplet charge at this point is given by<sup>2,3</sup>

$$z_R e = 8\pi \sqrt{\epsilon_0 \gamma R^3} \quad (1)$$

where  $z_R$  is the number of elementary charges  $e$ ,  $\epsilon_0$  is the permittivity of the vacuum,  $\gamma$  is the surface tension, and  $R$  is the

droplet radius. Jet fission at the Rayleigh limit produces daughter droplets that carry away a small percentage of the parent droplet mass but a disproportionately large amount of charge.<sup>4–9</sup> Successive evaporation/fission events ultimately lead to nanometer-sized droplets.<sup>4</sup> Throughout this process, differential evaporation leads to enrichment of the solvent component with the lowest vapor pressure, typically water.<sup>10,11</sup>

The mechanism of the final ESI step, i.e., the formation of gaseous analyte ions from highly charged nanodroplets, remains a matter of debate.<sup>12–17</sup> According to the charged residue model (CRM), evaporation to dryness releases the analyte, which retains some of the droplet's charge.<sup>4,18</sup> In contrast, the ion evaporation model (IEM) stipulates that charged analytes are ejected from the droplet surface by field emission.<sup>4,19–24</sup> Formation of gaseous analyte ions via the IEM leaves behind a solvent droplet, whereas this is not the case for the CRM. It has been suggested that large globular species such as dendrimers and natively folded proteins follow the CRM, whereas the IEM

**Received:** September 27, 2011

**Revised:** November 21, 2011

**Published:** December 12, 2011

applies to smaller analytes.<sup>4,21,25</sup> Support for the notion that the CRM is operative for large globular analytes comes from the observation of protonation states that are close to  $z_R$  of correspondingly sized water droplets.<sup>25–30</sup> However, it remains unclear whether this mechanism also applies to polymers that adopt extended conformations.<sup>31–33</sup> Recently developed hybrid models involving elements of both the CRM and the IEM have renewed the discussion of ESI mechanism(s).<sup>34,35</sup>

Molecular dynamics (MD) simulations represent an interesting approach for studies on the ESI process. Insights into the mechanisms whereby small solvated ions are released from nanodroplets come from a number of such investigations.<sup>11,36–45</sup> These studies support the view that small charge carriers such as  $\text{Na}^+$  and  $\text{NH}_4^+$  are ejected from the nanodroplet surface via thermally activated barrier crossing,<sup>11</sup> consistent with predictions of the IEM.<sup>4,19–24</sup> Several MD simulations were also conducted for nanodroplets containing macromolecular analytes,<sup>46–48</sup> but the implications of those studies for the ESI mechanism are less clear. Recent work by Consta suggests that sodiated polyethylene glycol gets ejected from charged nanodroplets via an IEM-like process.<sup>33</sup> Initial attempts from our laboratory to simulate the ESI process for polymer chains employed a minimalist approach, yielding data that do not necessarily reflect the behavior of aqueous systems.<sup>31</sup>

Building on those previous computational investigations,<sup>11,31,33,36–43,46–48</sup> the current work employs MD simulations with the aim of improving the understanding of macromolecular ESI. Solvent water and excess ions are treated using atomistic models.<sup>11,49</sup> As analytes, we employ polymer chains that are modeled on the basis of a coarse-grained framework.<sup>50,51</sup> Our polymer model draws on earlier polyampholyte studies,<sup>52,53</sup> and it follows a bead lattice strategy similar to approaches that have been widely used in the protein folding literature.<sup>54,55</sup> The method employed here aims to minimize the complexity of the overall system, while still allowing qualitative comparisons with experimental data.

From an ESI-MS practitioner's perspective, an important figure of merit is the ESI efficiency. In the context of the current work, we define this term as propensity of the polymer to emerge from the charged nanodroplet as a largely desolvated gas phase ion, regardless of mechanism. Polymers with low ESI efficiencies will tend to remain heavily solvated and/or trapped within their droplet prison.<sup>14</sup> Conversely, a high ESI efficiency entails rapid desolvation or efficient ejection from the droplet, thereby facilitating the acquisition of high quality mass spectra.<sup>56,57</sup>

Previous experimental studies indicate that the ESI efficiency of biomolecular analytes is greatly affected by (i) hydrophobicity and (ii) conformation.<sup>1,57–63</sup> The simulations of this work, therefore, focus on the behavior of polymer chains that exhibit different degrees of hydrophobicity and that are either folded (compact) or unfolded (extended). It would be fascinating to use MD simulations for describing the entire ESI process, from large droplets to nanometer-sized solvent clusters, and ultimately to desolvated gas-phase macromolecular ions. Unfortunately, the system size as well as the  $\mu\text{s}$ –ms time range<sup>56</sup> of these events represent major computational challenges. This work, therefore, focuses on the behavior of very small nanodroplets, using short simulation time windows on the order of 2.5 ns. Although this time frame is not quite long enough for observing the formation of fully desolvated gas phase polymer ions, interesting mechanistic features can, nonetheless, be uncovered. Polymers that are folded and hydrophilic behave in accordance with the CRM.

In contrast, species that are unfolded/hydrophobic exhibit IEM-like features. Our considerations are restricted to positively charged droplets, reflecting the prevalence of positive ion mode in most ESI-MS applications.

## METHODS

**Overall MD Strategy.** MD simulations were conducted in a vacuum environment with no boundary conditions, using C++ code developed in-house.<sup>11,42</sup> The droplet temporal evolution was modeled by integrating the classical equations of motion using the Verlet algorithm<sup>64</sup> with a time step of 2 fs. Each droplet contained 1000 water molecules and a polymer chain, as well as excess ammonium ions.  $\text{NH}_4^+$  was chosen because it represents a common charge carrier under ESI conditions.<sup>4</sup> Nanodroplets were generated from an initial cubic lattice, where individual molecules were placed in a random orientation. The polymer chain was placed at the center of this lattice. Using constant energy MD, this lattice was then coalesced into a compact droplet of approximately spherical geometry, with the polymer located close to the center. Droplet coordinates obtained using this coalescing procedure were then used as initial configurations for the actual MD simulations. For each of the four types of polymer chains that are discussed below, we conducted six simulation runs with different initial configurations (24 runs in total). The nanodroplets were subjected to Nose–Hoover thermalization<sup>65,66</sup> at 320 K for 80 ps. At  $t = 0$ , the simulations were switched to constant energy MD for  $\sim 2.5$  ns at  $T \approx 320$  K. Temperature was calculated by considering the contributions of all particles within 350 Å of the center of mass. As expected,<sup>56</sup> evaporative cooling leads to a gradual temperature decrease in constant energy mode. The magnitude of this effect is on the order of 10 K for 2.5 ns simulation runs. Illustrative temperature profiles are depicted in Figure S1 of the Supporting Information.

In MD simulation studies, it is customary to disregard data obtained during the initial thermalization period and to focus only on the constant energy regime. However, it will be seen that for some of the systems considered here, significant changes occur already during thermalization. For this reason, all data sets discussed below include the thermalization period (designated as –80 ps to  $t = 0$ ). Images were rendered using VMD.<sup>67</sup>

**Solvent Model.** Water was represented on the basis of the SPC/E model with an O–H bond distance of 1.0 Å and a H–O–H angle of 109.47°.<sup>49</sup> The pairwise interaction between  $\text{H}_2\text{O}$  molecules is given by a combination of LJ and Coulomb potentials.<sup>39</sup> LJ parameters for water are  $\sigma_{\text{OO}} = 3.166$  Å and  $\epsilon_{\text{OO}} = 0.6502$  kJ mol<sup>–1</sup>, with charges  $q_{\text{O}} = -0.8476$  e and  $q_{\text{H}} = 0.4238$  e. Ammonium ions were modeled with a N–H bond distance of 1.02 Å and a H–N–H angle of 109.47°. LJ parameters for  $\text{NH}_4^+$  are  $\sigma_{\text{NN}} = 3.45$  Å and  $\epsilon_{\text{NN}} = 0.7782$  kJ mol<sup>–1</sup>, with charges  $q_{\text{N}} = -0.8172$  e and  $q_{\text{H}} = 0.4543$  e.<sup>68</sup> Bond angles and bond lengths of water and ammonium were constrained using the SHAKE algorithm.<sup>69,70</sup> The same force field has been used in other recent ESI simulations, providing good agreement between MD results, continuum models, and experimental observations.<sup>11,38,39,42</sup>

**Polymer Model.** The coarse-grained model used here consists of a 27-bead chain that represents the macromolecule backbone, and an additional 26 beads representing side chains (Figure 1). Each bead has a mass of 16 amu, with Lennard-Jones parameters of  $\sigma = 4.0$  Å and  $\epsilon = 0.6502$  kJ mol<sup>–1</sup>. The beads fall into three categories, depending on their electric charge. Side chain beads

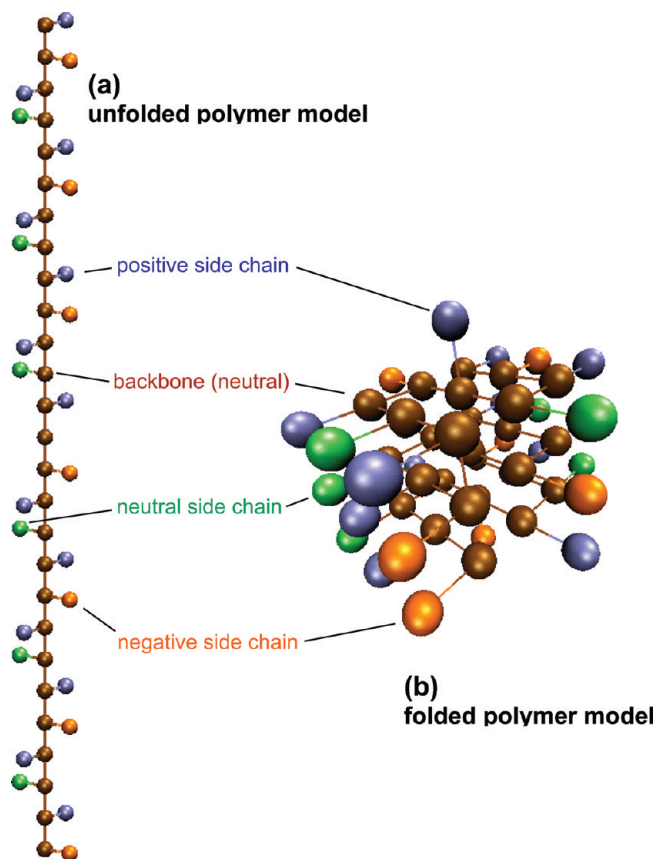


**Figure 1.** Representation of the coarse-grained polymer model used here, consisting of beads that represent backbone and side chain moieties. The backbone can either be unfolded (shown in a fully stretched conformation, panel a), or folded (b). Color coding: brown, neutral backbone; green, neutral side chain; light blue, positive side chain; orange, negative side chain.

**Table 1. Side Chain Charge Patterns for the Polymer Models Used in This Work<sup>a</sup>**

type	side chain charge pattern	net charge
hydrophobic	+ 0 0 0 + 0 0 0 + 0 0 0 X 0 +	+6
	0 0 0 0 + 0 0 0 0 +	
hydrophilic	+ - + 0 + - + 0 + - + 0 +	+6
	X - + 0 + - + 0 + - + 0 + -	

<sup>a</sup> Side chains carry either a positive elementary charge (+), a negative charge (-), or a zero charge (0). X indicates the lack of a side chain at backbone bead number 14.

can be positively (+1 e) or negatively charged (-1 e), or they can be neutral. Backbone beads in our model are neutral as well. It will be seen that positively and negatively charged beads tend to be strongly hydrated. Interactions with water are less favorable for neutral beads. We focus on two side chain patterns, both of which result in a net charge of +6 e (Table 1). The total number of charges is much lower for the first arrangement of Table 1, which encompasses six positive side chains and no negatively charged sites. This will be referred to as the hydrophobic side chain pattern. The second arrangement is designated as hydrophilic, reflecting the higher number of charges (13 positive and 7 negative side chains). We make the simplifying assumption that

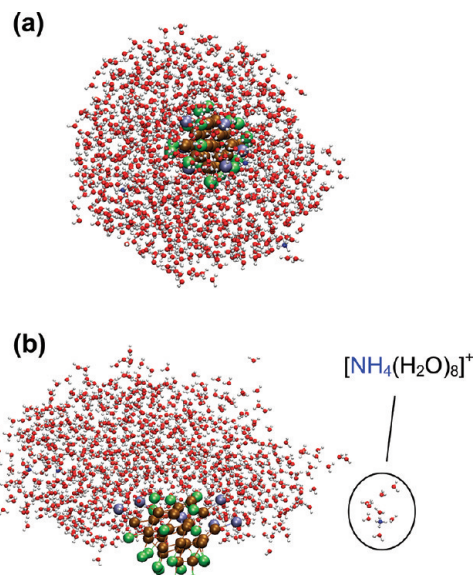


**Figure 2.** Illustrative MD simulation results for a folded/hydrophobic polymer at the onset of thermalization ( $t = -80$  ps, panel a), and at 284 ps (b). Color code as in Figure 1. In addition, white for hydrogen, red for oxygen, and dark blue for nitrogen. Note the ejection of a hydrated ammonium ion in (b). MD movies can be found in the Supporting Information.

the charges on the macromolecule remain constant during the simulation time window.

Two types of macromolecular conformations were investigated in this work, corresponding to the unfolded and the folded forms of the bead chain. The unfolded version (Figure 1a) represents a self-avoiding chain with unconstrained bond angles. Covalent linkages are described using a harmonic potential

$$U(r) = \frac{1}{2}k_s(r - r_0)^2 \quad (2)$$

with  $k_s = 4000$  kJ mol<sup>-1</sup> Å<sup>-2</sup>, and  $r_0 = 4.0$  Å. For folded macromolecules (Figure 1b), the backbone is arranged in a  $3 \times 3 \times 3$  cubic lattice. Side chains are attached to the 26 backbone entities that are located on the outside of this cube. The innermost backbone bead remains side-chain-free due to geometric constraints, which is why the model contains only 26 side chains for the 27 backbone beads. To prevent unfolding of the compact conformers during the simulations, spatially adjacent beads were linked by harmonic potentials (eq 2). These additional interactions ensure a relatively rigid shape for the cubic core, with only relatively minor contortions during the simulation time window.

The polymer model employed here (Figure 1) is not meant to represent a specific chemical species, but it shares several basic features with protein chains.<sup>71,72</sup> Specifically, proteins can adopt folded and unfolded structures. The solubility characteristics of proteins are largely governed by side chains, whereas the backbone is only moderately soluble in water.<sup>71</sup> Natively folded proteins have most of their nonpolar residues buried in a hydrophobic core that is inaccessible to the solvent. This core is surrounded by polar and charged residues that can favorably interact with water (analogous to the folded model conformation of Figure 1b). Unfolding of a globular protein greatly enhances its effective hydrophobicity because formerly buried nonpolar

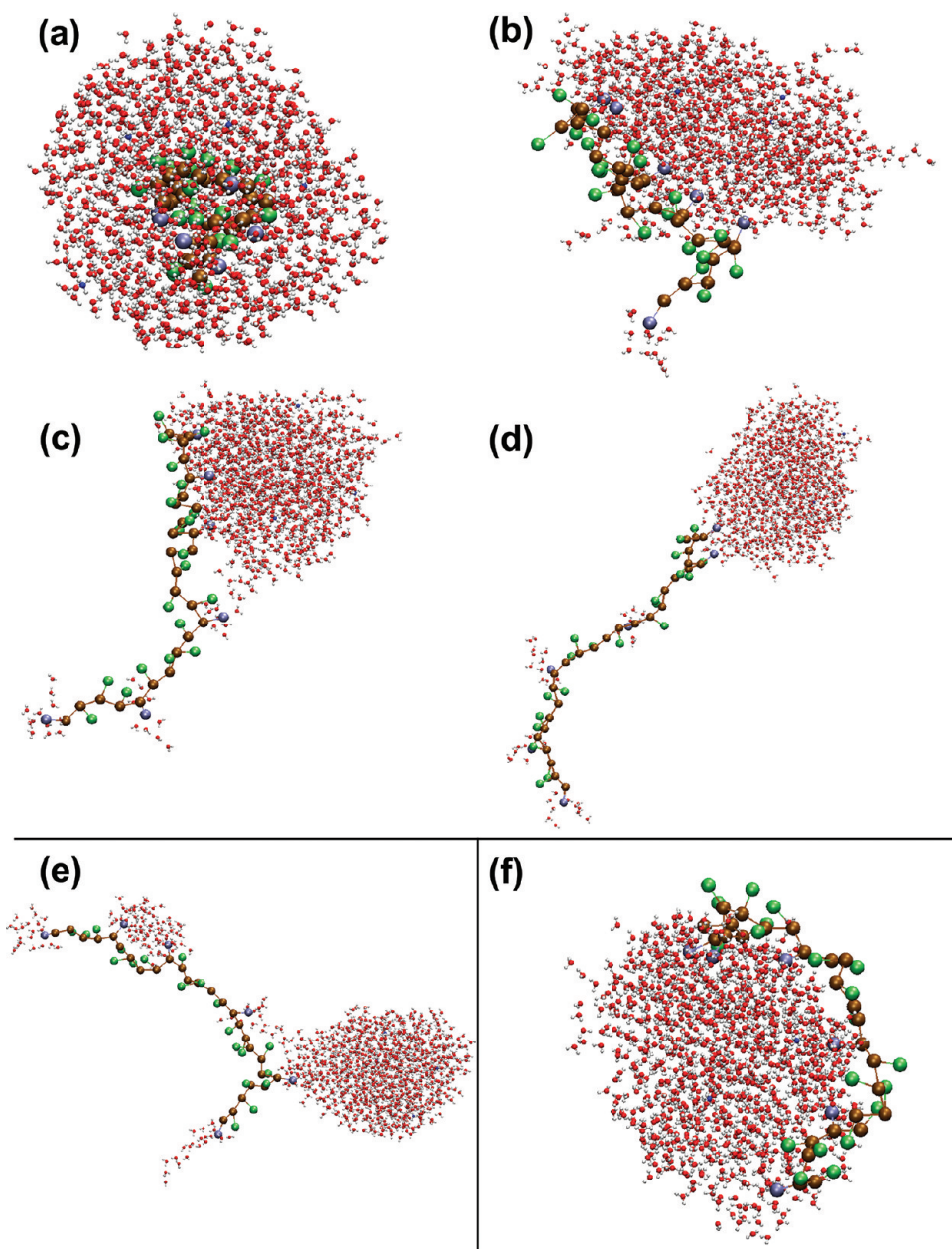


**Figure 3.** Simulation data from a MD run for an unfolded/hydrophobic polymer at time points  $-80$  ps (a),  $67$  ps (b),  $302$  ps (c),  $1147$  ps (d). Three of the six simulations on unfolded/hydrophobic polymer chains displayed this behavior. One of the runs produced the configuration of panel e at  $2468$  ps. Two of the runs resulted in a configuration illustrated in panel f for  $t = 2420$  ps. Color coding is identical to that in Figure 2.

residues become exposed to the solvent (Figure 1a).<sup>59,71,72</sup> Beyond these simple aspects, however, there are only limited similarities between our coarse-grained model and real proteins. Although the bond length of  $r_0 = 4.0$  Å corresponds to the spacing between adjacent polypeptide C $\alpha$  atoms,<sup>71</sup> the backbone beads of the model were not designed to mimic the behavior of a polyamide chain. Instead, the closely packed backbone beads represent the nonpolar core of the folded conformation (Figure 1b).

Nanometer-sized droplets encountered during the final stages of the ESI process are close to the Rayleigh limit.<sup>4,25–29</sup> The droplets considered in this work have radii on the order of 2 nm. The initial excess charge of the droplets discussed below was chosen to be  $+10$  e, which corresponds to  $\sim 90\%$  of  $z_R$  (eq 1).<sup>73</sup>

These ten elementary charges are composed of  $+6$  e on the polymer side chains and four ammonium ions.

**Mass Spectrometry.** ESI mass spectra of horse heart myoglobin (Sigma, St. Louis, MO) were recorded in aqueous solution at a protein concentration of  $10 \mu\text{M}$  and in the presence of  $50 \text{ mM}$  ammonium acetate. The total ion current from  $65$  three second scans was integrated. Data for the folded protein (holo-myoglobin) were acquired at pH 7. For measurements on the unfolded protein (apo-myoglobin), the solution was acidified to pH 2 with formic acid. There was no indication of protein precipitation under these conditions. The data were acquired at a solution flow rate of  $5 \mu\text{L min}^{-1}$  on a Q-TOF Ultima mass spectrometer (Waters, Manchester, UK) equipped with a Z-spray ESI source.

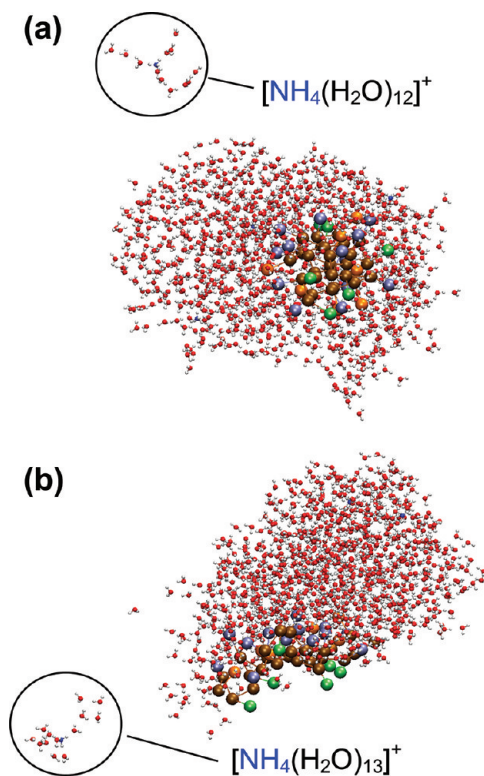


**Figure 4.** Illustrative MD simulation results for a folded/hydrophilic polymer at 586 ps (a) and an unfolded/hydrophilic polymer at 328 ps (b). Both panels illustrate the ejection of a hydrated ammonium ion. Color coding is identical to that in Figure 2.

## RESULTS AND DISCUSSION

For modeling the polymer behavior under ESI conditions, MD simulations were conducted following the procedures outlined above. Each aqueous nanodroplet initially contained one polymer chain and four excess ammonium ions. Ejection of solvated  $\text{NH}_4^+$  from the nanodroplets occurs at an average rate of  $\sim 1.3 \text{ ns}^{-1}$  for all the scenarios considered below. These ion ejection events are well described by the IEM, as discussed in detail elsewhere.<sup>11</sup> The focus of the current work is on the behavior of the macromolecular analyte. We will initially consider hydrophobic polymer chains, and then move on to hydrophilic systems. The side chain patterns for these two cases are depicted in Table 1. Folded and unfolded conformations will be studied in each case (Figure 1). MD movies for the various scenarios discussed below can be found in the Supporting Information.

**Hydrophobic Polymer Behavior.** A droplet containing a folded/hydrophobic polymer chain is depicted in Figure 2 for two different time points. At the onset of the simulation run ( $t = -80 \text{ ps}$ , Figure 2a), the polymer is positioned near the center of the droplet. Structural rearrangement of the system rapidly moves the analyte to the droplet surface (depicted for  $t = 284 \text{ ps}$  in Figure 2b). The macromolecule maintains this position for the remainder of the  $\sim 2.5 \text{ ns}$  simulation time window. In this metastable arrangement, the six positively charged side chains are oriented toward the droplet interior where they are extensively solvated. Most of the hydrophobic side chains (green) point toward the vapor phase. The droplet maintains a highly dynamic structure throughout the simulation period, with occasional ejection of hydrated ammonium ions (Figure 2b) and

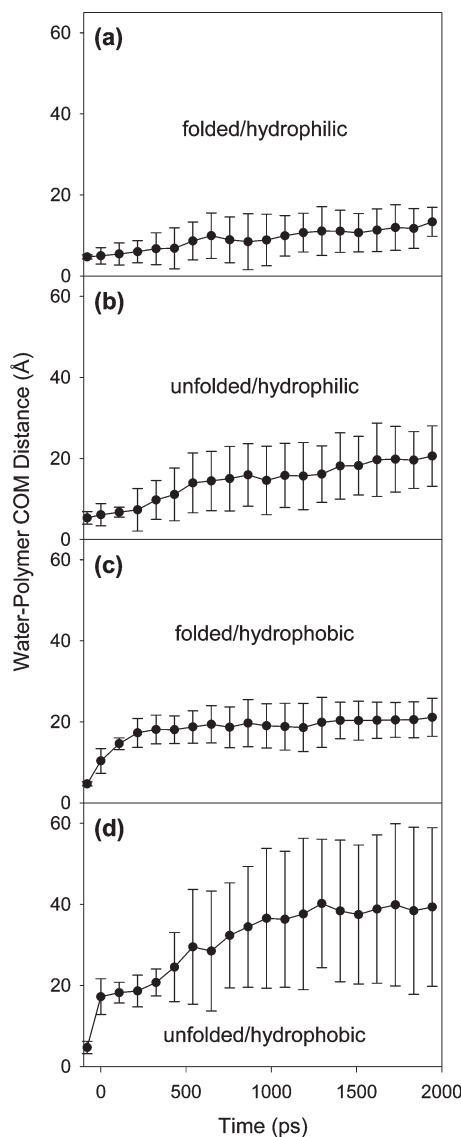


**Figure 5.** Temporal development of the average center-of-mass (COM) distance between solvent and polymer. Panels a–d refer to the four different polymer models (folded/hydrophilic, unfolded/hydrophilic, folded/hydrophobic, and unfolded/hydrophobic), as indicated in the figure. Each data point represents an average of six simulation runs. Error bars represent standard deviations. The y axes in all four panels are scaled equally to facilitate the comparison of data. COM calculations were performed by including all molecules within a 130 Å radius.

evaporation of individual water molecules. All six runs for folded/hydrophobic polymer chains exhibited a behavior very similar to that illustrated in Figure 2.

MD runs for unfolded/hydrophobic polymer chains display a dramatically different behavior. Figure 3a–d illustrates a sequence of events observed for three of the six simulations. At  $-80 \text{ ps}$  the macromolecule is close to the droplet center (Figure 3a). During the thermalization period, the chain starts to uncoil, and by  $0 \text{ ps}$ , it has pushed itself to the surface. Shortly thereafter, the first charged side chain starts to detach itself from the droplet, illustrated in Figure 3b for  $t = 67 \text{ ps}$ . The other charged side chains remain solvated by water close to the droplet periphery at this time point. By  $302 \text{ ps}$ , a second charged side

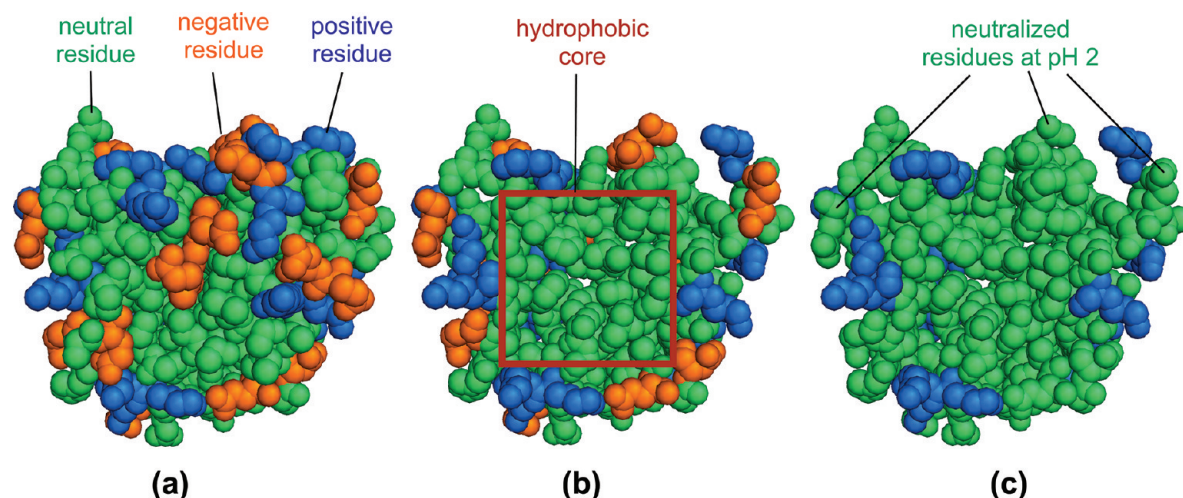


**Figure 6.** X-ray structure of myoglobin<sup>75</sup> in space fill representation. Positively and negatively charged sites, as well as neutral residues are depicted using the same colors as those in Figure 1. (a) Overview of the whole protein, revealing the accumulation of charged sites on the surface at pH 7. (b) Slab representation at pH 7, obtained by removing one layer of residues facing the observer. The clustering of nonpolar residues in the protein interior (hydrophobic core) is highlighted by a brown square.<sup>75</sup> Note the parallels of this scenario to the model of Figure 1b. (c) Same as in panel b, but after acid-induced charge neutralization of all carboxylic acid groups. Note that this acidification will be followed by unfolding of the protein chain (not shown in panel c).

chain is detached, while another one is on the verge of detachment (Figure 3c). This process continues until the entire polymer chain has been expelled from the droplet but remains connected to the surface through hydration of the last two charged side chains ( $t = 1147$  ps, Figure 3d). Expelled charge sites retain solvation by small water clusters (Figure 3d). The system remains in this metastable state for at least 2.5 ns, which is the longest time point explored in this study. Recent MD simulations on the expulsion of sodiated polyethylene glycol from water droplets showed a very similar behavior, with detachment of the polymer chain from the droplet after  $\sim 18$  ns.<sup>33</sup>

As noted above, the unfolded/hydrophobic polymer behavior illustrated in Figure 3a–d was observed for three of the six simulation runs. In one case, the expulsion followed a somewhat different pattern, with a residual polymer-droplet connection in the center of the chain rather than at the chain terminus (Figure 3e,  $t = 2468$  ps).

Two of the six unfolded/hydrophobic simulation runs did not lead to expulsion of the polymer. Instead, they produced configurations where the chain was wrapped around the droplet periphery, with charged side chains that remained firmly rooted in the aqueous phase (Figure 3f,  $t = 2420$  ps). The lack of polymer expulsion in these two cases can be attributed to the ejection of two ammonium ions during the simulation runs. This loss of excess charge from the droplet lowers the Coulombic driving force for polymer expulsion. In contrast, the four simulation runs that did result in unfolded/hydrophobic polymer expulsion (as in Figure 3d or e) showed ejection of either zero  $\text{NH}_4^+$  (3 runs) or one  $\text{NH}_4^+$  (one run). Taken together, our data imply that polymer expulsion from the droplet is mediated by an interplay of hydrophobic and electrostatic factors.

**Hydrophilic Polymer Behavior.** MD simulations conducted on folded/hydrophilic macromolecules reveal a strong tendency of the polymer to remain buried deeply within the droplet during the entire simulation window. As an example, Figure 4a depicts a snapshot taken at  $t = 586$  ps. In the case of the unfolded/hydrophilic polymer, the chain moves somewhat closer to the

droplet surface, such that several nonpolar side chains can protrude into the vapor phase, while charged sites remain extensively hydrated (Figure 4b,  $t = 328$  ps). Once again, the configurations of Figure 4 represent metastable scenarios that display only relatively small changes during the remainder of the simulation window. None of the hydrophilic polymer chains showed any tendency to undergo expulsion from the droplet.

**ESI Efficiency.** In an attempt to quantify the desolvation propensity of the four different polymer chain types, we calculated the average center-of-mass (COM) distance between water and macromolecule as a function of time (Figure 5). All four profiles obtained in this way originate at COM distances around 4 Å, representing the initial situation where the polymer is enclosed by solvent within the droplet at  $t = -80$  ps. Folded/hydrophilic chains maintain very low COM distances throughout the entire time window (Figure 5a). Desolvation is slightly enhanced for the unfolded/hydrophilic scenario where the average COM distance rises to ca. 20 Å (Figure 5b). A similar behavior is observed for folded/hydrophobic polymers (Figure 5c). These values correspond to macromolecule positions at the liquid/vapor interface, keeping in mind that the droplet radius is also  $\sim 20$  Å. The most dramatic behavior is seen for unfolded/hydrophobic chains. In this case, the COM distance increases to roughly 40 Å within 1 ns, reflecting the prevalence of trajectories where the polymer chain gets rapidly expelled from the droplet (Figure 5d).

In the Introduction, we defined ESI efficiency as the propensity of the polymer to emerge from the charged droplet as a largely desolvated gas phase ion. The limited time window accessible in our simulations precludes the formation of completely free gas phase polymer ions. Nonetheless, it is clear from our data that unfolded/hydrophobic macromolecules (Figure 5d) shed their surrounding droplet environment most readily, which should translate into the highest ESI efficiency. Conversely, folded/hydrophilic chains are expected to show the lowest ESI efficiencies because they remain most deeply buried within the droplet (Figure 5a).

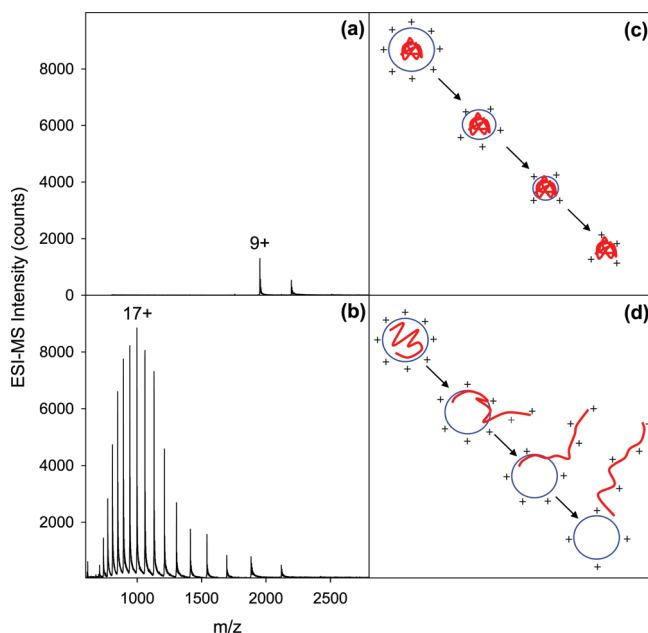


**Figure 7.** Illustration of different macromolecular ESI mechanisms. Panels a and b show ESI mass spectra of myoglobin recorded at pH 7 (a) and of the acid-unfolded protein at pH 2 (b). The y axes in panels a and b are scaled equally to emphasize the intensity difference of the spectra. (c) Schematic cartoon, depicting the formation of a gas phase macromolecule via the CRM. This mechanism is proposed to be operative for folded polypeptides with a hydrophilic exterior (such as folded myoglobin, panel a). The key factor responsible for the formation of gas-phase protein ions in panel c is slow solvent evaporation to dryness. (d) Hydrophobically assisted IEM-like mechanism. This scenario applies to the formation of gas phase ions in the case of unfolded/hydrophobic polymers (such as acid-unfolded myoglobin, panel b). The mechanism in panel d involves rapid expulsion of the protein from the surface of an intact droplet.

**Comparison With Experimental Data.** The predictions of our model regarding the ESI efficiency were assessed in measurements on myoglobin, a commonly used test protein in ESI-MS.<sup>74</sup> Folded myoglobin at pH 7 possesses numerous charged sites. These include the amino terminus, 19 Lys, and 2 Arg (22 positive charges), as well as 13 Glu, 8 Asp, 2 heme propionates, and the carboxyl terminus (24 negative charges). X-ray data reveal that in folded myoglobin, all of these charges are exposed to the solvent (Figure 6a).<sup>75</sup> In contrast, many neutral residues are buried without solvent access. A large number of these buried sites are nonpolar, giving rise to the formation of a hydrophobic core (Figure 6b).<sup>75</sup> In qualitative terms, therefore, folded myoglobin at pH 7 resembles our coarse-grained folded/hydrophilic model, where a closely packed core of neutral beads is surrounded by a large number of charged moieties (Figures 1b and 6b).

Exposure of myoglobin to pH 2 has two major consequences: (i) all of the negative charges are neutralized by protonation ( $-\text{COO}^- + \text{H}^+ \rightarrow -\text{COOH}$ , Figure 6c),<sup>71</sup> and (ii) the protein undergoes unfolding, thereby exposing many formerly buried nonpolar residues to the solvent.<sup>76</sup> Taken together, these two factors dramatically enhance the effective hydrophobicity of the unfolded protein.<sup>31,59,74</sup> Myoglobin at pH 2, therefore, shares characteristics with our unfolded/hydrophobic polymer model, i.e., an extended conformation, relatively few charged sites, and a large number of solvent-exposed neutral moieties.

ESI-MS analysis of myoglobin at pH 7 results in a fairly low signal intensity (Figure 7a). A striking enhancement by more than 1 order of magnitude in total ion count is seen upon acidification of the protein to pH 2 (Figure 7b). This intensity enhancement is in qualitative agreement with the predictions of our MD simulations, where unfolded/hydrophobic chains are readily expelled from the droplet (Figure 5d) and where desolvation is inefficient for folded/hydrophilic chains (Figure 5a). Inefficient desolvation and low analyte ejection rates from droplets are known to generally reduce signal intensities in ESI-MS.<sup>56,57</sup>

## CONCLUSIONS

In this study, we explored the behavior of charged aqueous nanodroplets containing ammonium ions and a model polymer. Possible avenues that would allow the droplets to lower their electrostatic energy include  $\text{NH}_4^+$  emission, as well as partial or complete ejection of the macromolecule. The rates of these processes are governed by an interplay of charge repulsion, solvent–solvent interactions, and solvent–solute interactions. Focusing on the two most extreme scenarios, we will briefly examine the implications of our findings for the mechanism by which gaseous macromolecular ions are formed from ESI droplets.

The most dramatic time-dependent events are observed for unfolded/hydrophobic polymers. In this case, the chain gets expelled from the droplet in a stepwise sequential fashion, one charged residue at a time. This expulsion is largely driven by Coulomb repulsion between cationic side chains and excess charge carriers in the droplet. In addition, the process is facilitated by unfavorable interactions between water and hydrophobic parts of the polymer.<sup>77</sup> A synergistic interplay between electrostatic forces and hydrophobicity during ion emission has previously been envisioned by others.<sup>1,57</sup> The expulsion of unfolded/hydrophobic chains tends to proceed via tadpole-shaped structures that consist of a water droplet body and an extended polymer tail (Figure 3c,d). Thermal activation will ultimately trigger complete separation of the polymer from the droplet,<sup>33</sup> thereby giving rise to the formation of a free gas phase macromolecular ion. Clearly, this sequence of events (Figure 3a–d) bears analogies to the IEM,<sup>4,11,19–24</sup> where ions are ejected from the surface of an intact droplet by field emission. However, a central element of many previous IEM studies is the assumption of a single free energy barrier that separates the droplet-bound ion from the free gas phase state. In other words, the classical IEM envisions ion ejection to be a one-step event.<sup>4,11,19–24</sup> In contrast, this study as well as previous work<sup>33</sup> reveals that the expulsion of unfolded/hydrophobic polymer chains occurs in a gradual, multistep manner (Figure 3a–d). Overall, we conclude that gas phase ion formation for unfolded/hydrophobic macromolecules is most appropriately described as a hydrophobically assisted IEM-like process. A cartoon representation of this mechanism is depicted in Figure 7d. We suggest that this mechanism is operative for proteins such as acid-unfolded myoglobin (Figure 7b).

The situation is completely different for folded/hydrophilic macromolecules. In this case, the polymer chain remains close to the center of the droplet, where solvation of charged side chains by water is maximized. This extensive solvation makes analyte ejection from the droplet surface a highly unfavorable process. Instead, release into the gas phase will only be possible via the

CRM, where solvent evaporation eventually leaves behind a dried-out macromolecule. Shrinkage of the droplet during this drying-out process will be accompanied by ejection of charge carriers (e.g., Figure 4), such that the macromolecule/solvent system remains close to the Rayleigh limit at all times.<sup>35</sup> Ultimately, this scenario will produce free macromolecular ions with charges close to  $z_R$ , in agreement with experimental observations.<sup>25–29</sup> Figure 7c shows a cartoon, representing the CRM steps that lead to formation of gas phase ions for a folded/hydrophilic polymer (such as myoglobin at pH 7, Figure 7a).

The release of folded/hydrophilic polymers into the gas phase via the CRM involves extensive solvent evaporation, which is a relatively slow ( $\sim\mu\text{s}$ ) process.<sup>4</sup> In contrast, our simulations reveal that IEM-like ejection of unfolded/hydrophobic chains occurs several orders of magnitude faster. This increased rate translates into a higher ESI efficiency for unfolded/hydrophobic macromolecules, a prediction that is confirmed by the ion intensity differences in the experimental data of Figure 7a,b. Overall, our simulations provide a mechanistic explanation for the well-known fact that ESI-MS signal intensities can be enhanced by both addition of acid and the attachment of hydrophobic moieties to the analyte.<sup>57,62,63</sup>

In future work, it will be interesting to conduct ESI simulations on larger water droplets containing more realistic polymer models than those employed in the current study. It is hoped that it will also be possible to incorporate proton transfer events, with the aim of reproducing changes in protein charge state during ESI (as seen in the experimental data of Figure 7a,b).<sup>74</sup> We envision that the higher charge states of the unfolded protein are the result of proton transfer during expulsion from the droplet (Figure 7d). This process may be analogous to charge partitioning phenomena that occur during the dissociation of protein complexes in the gas phase.<sup>78</sup>

## ■ ASSOCIATED CONTENT

**5 Supporting Information.** Examples of MD trajectories (.mpg movies) for the four polymer scenarios investigated in this work: folded/hydrophilic, folded/hydrophobic, unfolded/hydrophilic, and unfolded/hydrophobic. All movies cover the time range from  $-80$  ps to  $1.1$  ns. Also included are temperature profiles for two simulation runs that illustrate the occurrence of evaporative cooling. This material is available free of charge via the Internet at <http://pubs.acs.org>.

## ■ AUTHOR INFORMATION

### Corresponding Author

\*Tel: (519) 661-2111, ext. 86313. Fax: (519) 661-3022. E-mail: konerman@uwo.ca. Webpage: <http://publish.uwo.ca/~konerman>.

## ■ ACKNOWLEDGMENT

This work was financially supported by the Natural Sciences and Engineering Research Council of Canada (NSERC), The University of Western Ontario, and the Canada Research Chairs Program. MD simulations were carried out using SHARCNET ([www.sharcnet.ca](http://www.sharcnet.ca)). We thank Dr. Jingxi Pan for help with acquisition of the protein mass spectra of Figure 7.

## ■ REFERENCES

- (1) Fenn, J. B. *Angew. Chem., Int. Ed.* **2003**, *42*, 3871–3894.
- (2) Kebarle, P.; Peschke, M. *Anal. Chim. Acta* **2000**, *406*, 11–35.
- (3) Rayleigh, L. *Philos. Mag.* **1882**, *14*, 184–186.
- (4) Kebarle, P.; Verkerk, U. H. *Mass Spectrom. Rev.* **2009**, *28*, 898–917.
- (5) Gu, W.; Heil, P. E.; Choi, H.; Kim, K. *Appl. Phys. Lett.* **2007**, *91*, 064104.
- (6) Gomez, A.; Tang, K. *Phys. Fluids* **1994**, *6*, 404–414.
- (7) Duft, D.; Achtzehn, T.; Muller, R.; Huber, B. A.; Leisner, T. *Nature* **2003**, *421*, 128.
- (8) Li, D.; Marquez, M.; Xia, Y. *Chem. Phys. Lett.* **2007**, *445*, 271–275.
- (9) Konermann, L. *J. Am. Soc. Mass Spectrom.* **2009**, *20*, 496–506.
- (10) Samalikova, M.; Grandori, R. *J. Am. Chem. Soc.* **2003**, *125*, 13352–13353.
- (11) Ahadi, E.; Konermann, L. *J. Am. Chem. Soc.* **2011**, *133*, 9354–9363.
- (12) Spencer, E. A. C.; Ly, T.; Julian, R. K. *Int. J. Mass Spectrom.* **2008**, *270*, 166–172.
- (13) Fenn, J. B. *J. Am. Soc. Mass Spectrom.* **1993**, *4*, 524–535.
- (14) Fenn, J. B.; Rosell, J.; Meng, C. K. *J. Am. Soc. Mass Spectrom.* **1997**, *8*, 1147–1157.
- (15) Nguyen, S.; Fenn, J. B. *Proc. Natl. Acad. Sci. U.S.A.* **2007**, *104*, 1111–1117.
- (16) Wilm, M. *Mol. Cell. Proteomics* **2011**, *10*, 0094071–0094078.
- (17) Liuni, P.; Wilson, D. *J. Expert Rev. Proteomics* **2011**, *8*, 197–209.
- (18) Dole, M.; Mack, L. L.; Hines, R. L.; Mobley, R. C.; Ferguson, L. D.; Alice, M. B. *J. Chem. Phys.* **1968**, *49*, 2240–2249.
- (19) Thomson, B. A.; Iribarne, J. V. *J. Chem. Phys.* **1979**, *71*, 4451.
- (20) Iribarne, J. V.; Thomson, B. A. *J. Chem. Phys.* **1976**, *64*, 2287–2294.
- (21) Gamero-Castaño, M.; de la Mora, F. *J. Mass Spectrom.* **2000**, *35*, 790–803.
- (22) Tang, L.; Kebarle, P. *Anal. Chem.* **1993**, *65*, 3654–3668.
- (23) Labowsky, M. *Rapid Commun. Mass Spectrom.* **2010**, *24*, 3079–3091.
- (24) Loscertales, I. G.; de la Mora, J. F. *J. Chem. Phys.* **1995**, *103*, 5041–5060.
- (25) Iavarone, A. T.; Williams, E. R. *J. Am. Chem. Soc.* **2003**, *125*, 2319–2327.
- (26) de la Mora, F. *J. Anal. Chim. Acta* **2000**, *406*, 93–104.
- (27) Felitsyn, N.; Peschke, M.; Kebarle, P. *Int. J. Mass Spectrom.* **2002**, *219*, 39–62.
- (28) Nesatyy, V. J.; Suter, M. J.-F. *J. Mass Spectrom.* **2004**, *39*, 93–97.
- (29) Kaltashov, I. A.; Mohimen, A. *Anal. Chem.* **2005**, *77*, 5370–5379.
- (30) Heck, A. J. R.; Van den Heuvel, R. H. H. *Mass Spectrom. Rev.* **2004**, *23*, 368–389.
- (31) Konermann, L. *J. Phys. Chem. B* **2007**, *111*, 6534–6543.
- (32) Testa, L.; Brocca, S.; Grandori, R. *Anal. Chem.* **2011**, *83*, 6459–6463.
- (33) Consta, S.; Chung, J. K. *J. Phys. Chem. B* **2011**, *115*, 10447–10455.
- (34) Wang, G.; Cole, R. B. *Anal. Chim. Acta* **2000**, *406*, 53–65.
- (35) Hogan, C. J.; Carroll, J. A.; Rohrs, H. W.; Biswas, P.; Gross, M. L. *Anal. Chem.* **2009**, *81*, 369–377.
- (36) Znamenskiy, V.; Marginean, I.; Vertes, A. *J. Phys. Chem. A* **2003**, *107*, 7406–7412.
- (37) Marginean, I.; Znamenskiy, V.; Vertes, A. *J. Phys. Chem. B* **2006**, *110*, 6397–6404.
- (38) Ichiki, K.; Consta, S. *J. Phys. Chem. B* **2006**, *110*, 19168–19175.
- (39) Consta, S.; Mainer, K. R.; Novak, W. *J. Chem. Phys.* **2003**, *119*, 10125–10132.
- (40) Caleman, C.; van der Spoel, D. *Phys. Chem. Chem. Phys.* **2007**, *9*, 5105–5111.
- (41) Iyengar, S. S.; Day, T. J. F.; Voth, G. A. *Int. J. Mass Spectrom.* **2005**, *241*, 197–204.
- (42) Ahadi, E.; Konermann, L. *J. Am. Chem. Soc.* **2010**, *132*, 11270–11277.
- (43) Caleman, C.; Hub, J. S.; van Maaren, P. J.; van der Spoel, D. *Proc. Natl. Acad. Sci. U.S.A.* **2011**, *108*, 6838–6842.
- (44) Luedtke, W. D.; Landmann, U.; Chiu, Y.-H.; Levandier, D. J.; Dressler, R. A.; Sok, S.; Gordon, M. S. *J. Phys. Chem. A* **2008**, *112*, 9628–9649.
- (45) Daub, C. D.; Cann, N. M. *Anal. Chem.* **2011**, *83*, 8372–8376.

- (46) Steinberg, M. Z.; Breuker, K.; Elber, R.; Gerber, R. B. *Phys. Chem. Chem. Phys.* **2007**, *9*, 4690–4697.
- (47) Consta, S. *J. Phys. Chem. B* **2010**, *114*, 5263–5268.
- (48) Patriksson, A.; Marklund, E.; van der Spoel, D. *Biochemistry* **2007**, *46*, 933–945.
- (49) Berendsen, H. J. C.; Grigera, J. R.; Straatsma, T. P. *J. Phys. Chem.* **1987**, *91*, 6269–6271.
- (50) Bond, P. J.; Holyoake, J.; Ivetac, A.; Khalid, S.; Sansom, M. S. P. *J. Struct. Biol.* **2007**, *157*, 593–605.
- (51) Srinivas, G.; Discher, D. E.; Klein, M. L. *Nat. Mater.* **2004**, *3*, 638–644.
- (52) Higgs, P. G.; Joanny, J.-F. *J. Chem. Phys.* **1991**, *94*, 1543–1554.
- (53) Sodemann, T.; Schiessel, H.; Blumen, A. *Phys. Rev. E* **1998**, *57*, 2081–2090.
- (54) Dobson, C. M.; Sali, A.; Karplus, M. *Angew. Chem., Int. Ed.* **1998**, *37*, 868–893.
- (55) Dill, K. A.; Chan, H. S. *Nat. Struct. Biol.* **1997**, *4*, 10–19.
- (56) Kebarle, P.; Tang, L. *Anal. Chem.* **1993**, *65*, 972A–986A.
- (57) Cech, N. B.; Enke, C. G. *Mass Spectrom. Rev.* **2001**, *20*, 362–387.
- (58) Null, A. P.; Nepomuceno, A. I.; Muddiman, D. C. *Anal. Chem.* **2003**, *75*, 1331–1339.
- (59) Kuprowski, M. C.; Konermann, L. *Anal. Chem.* **2007**, *79*, 2499–2506.
- (60) Chalcraft, K. R.; Lee, R. C., M.; Britz-McKibbin, P. *Anal. Chem.* **2009**, *81*, 2506–2515.
- (61) Oss, M.; Krueve, A.; Herodes, K.; Leito, I. *Anal. Chem.* **2010**, *82*, 2865–2872.
- (62) Walker, S. H.; Lilley, L. M.; Enamorado, M. F.; Comins, D. L.; Muddiman, D. C. *J. Am. Soc. Mass Spectrom.* **2011**, *22*, 1309–1317.
- (63) Kulevich, S. E.; Gloria Kreitinger, B. F.; Smith, L. M. *Anal. Chem.* **2010**, *82*, 10135–10142.
- (64) Verlet, L. *Phys. Rev.* **1967**, *159*, 98–103.
- (65) Nose, S. *Mol. Phys.* **1984**, *52*, 255–268.
- (66) Hoover, W. G. *Phys. Rev. A* **1985**, *31*, 1695–1697.
- (67) Humphrey, W.; Dalke, A.; Schulten, K. *J. Mol. Graphics* **1996**, *14*, 33–38.
- (68) Chang, T.-M.; Dang, L. X. *J. Chem. Phys.* **2003**, *118*, 8813–8820.
- (69) Allen, M. P.; Tildesley, D. J. *Computer Simulation of Liquids*; Clarendon Press: Oxford, U.K., 1987.
- (70) Forester, T. R.; Smith, W. *J. Comput. Chem.* **1998**, *19*, 102–111.
- (71) Creighton, T. E. *Proteins*; W. H. Freeman & Co: New York, 1993.
- (72) Fersht, A. R. *Structure and Mechanism in Protein Science*; W. H. Freeman & Co.: New York, 1999.
- (73) Ahadi, E.; Konermann, L. *J. Phys. Chem. B* **2009**, *113*, 7071–7080.
- (74) Dobo, A.; Kaltashov, I. A. *Anal. Chem.* **2001**, *73*, 4763–4773.
- (75) Evans, S. V.; Brayer, G. D. *J. Mol. Biol.* **1990**, *213*, 885–897.
- (76) Eliezer, D.; Yao, J.; Dyson, H. J.; Wright, P. E. *Nat. Struct. Biol.* **1998**, *5*, 148–155.
- (77) Chandler, D. *Nature* **2007**, *445*, 831–832.
- (78) Sciuto, S. V.; Liu, J.; Konermann, L. *J. Am. Soc. Mass Spectrom.* **2011**, *22*, 1679–1689.